J. Plasma Fusion Res. SERIES, Vol. 5 (2002) 297–301

High Power ICRF Heating in the 4th Experimental in LHD

YAMAMOTO Taroh, KUMAZAWA Ryuhei[1], WATARI Tetsuo[1], MUTOH Takashi[1],
SEKI Tetsuo[1], SAITO Kenji, TORII Yuki, TAKEUTI Norio,
SASAO Mamiko[1], ISOBE Mitsutaka[1], OSAKABE Masaki[1] and LHD Experiment Group[1]
Nagoya University, Nagoya 464-8603, Japan
[1] National Institute for Fusion Science, Toki 509-5292 Japan

(Received: 14 December 2001 / Accepted: 5 July 2002)

Abstract

The utility of ICRF (Ion Cyclotron Range of Frequency) heating in the Large Helical Device (LHD) was demonstrated in the third campaign, carried out in 1999. This paper summarizes the investigations in 2000 focusing on the optimization of ICRF heating, in which scans of the magnetic field strength and the magnetic axis position were made. In the scan of the magnetic field, the optimized ICRF heating performance was obtained when the minority cyclotron resonance was located at the saddle point of the mod-B surface. Under this condition, the highest electron density of 2.7×10^{19} m^{-3} was sustained at a power level of 1.5 MW with ICRF heating only. In the scan of the magnetic axis, better performances of ICRF heating were obtained in the inward shifted configuration than in the outward shifted configuration. The difference in performance between the two cases was studied in terms of the difference of confinement of the high-energy ions as well as that of the bulk plasma.

Keywords:
ICRF heating, LHD, optimization, magnetic configuration

1. Introduction

ICRF heating is now one of the established heating schemes in tokamaks. However, its application to helical systems is not so straightforward and efforts have been made to establish it in helical systems [1-4]. The experimental results in the LHD [5] in the 3rd campaign provide a more advanced demonstration of the ICRF heating in the helical system than those in previous experiments, due to the high plasma stored energy attained and the overcoming of impurity problems [6,7].

Various working hypotheses were proposed as reasons for the success of the ICRF experiment in the third campaign and some of them have been introduced in previous publications [8]. The alignment of the flux surfaces on the drift orbits of the trapped particles due to the adopted magnetic axis shift has been pointed out as a possible candidate of confinement improvement [8,9].

Corresponding author's e-mail: tyamamo@nifs.ac.jp

The major achievement of ICRF heating in the fourth campaign was the injection of 2.7 MW of power, doubling the previous record. This paper limits its main scope to the associated optimization of ICRF heating and describes the performance of ICRF heating, which depends on the magnetic configuration and its strength: In Sec. **2**, the optimum heating condition for ICRF heating is identified by sweeping the magnetic field strength. In Sec. **3**, two discharges with different magnetic axes are compared and the differences in the behavior of high-energy ions are discussed. In Sec. **4**, the results obtained are discussed and summarized.

2. Dependence of the Heating Efficiency on the Magnetic Field Intensity

In the minority heating regime, a plasma consisting

of helium ions and hydrogen ions was heated. The former is the majority species and the latter is the minority species. The highest available magnetic field intensity on the magnetic axis of the LHD is B_t~2.9 T. The locations of resonance layers and cutoff layers are shown in Fig. 1. The calculation was made with the magnetic axis at R_{ax} = 3.6 m, magnetic field strength B_t = 2.75 T, the applied frequency f = 38.47 MHz, the line-averaged electron density n_e = 1×10^{19} m^{-3}, and the minority concentration ratio n_H/n_e = 0.05.

The performance of the ICRF heating is considered to depend on the location of the ion cyclotron resonance layer, with which the propagation and the absorption of the fast wave are characterized. Figure 2 shows the dependence of the plasma stored energy and the line-averaged electron density on the magnetic field strength. The data were taken from the discharges sustained by ICRF heating only, in the power range of 1.4~1.6 MW. Figure 2(a) shows that the maximum plasma stored energy was obtained at B_t = 2.75 T [6]. Under this condition, the ion cyclotron resonance layer was located so as to cross the saddle point area of the mod-B surface. The ICRF power may be absorbed effectively via cyclotron damping because of the gentle gradient of the magnetic field strength there. Figure 2(b) shows that the electron density attains its maximum value also at B_t = 2.75 T, reaching 2.7×10^{19} m^{-3}. The time evolutions of the plasma stored energy, the ICRF heating power, the line-averaged electron density and the radiated power are shown in Fig. 3. In this discharge the ICRF heating power was 1.5 MW. The line-averaged electron density was increased gradually with the increase of the introduced helium gas. The radiated power increased with the electron density up to 500 kW, which was 33 %

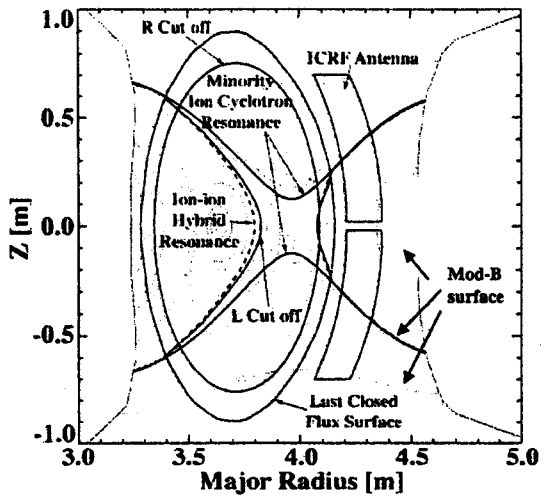

Fig. 1 The locations of resonance layers and cut-off layers in front of the ICRF antenna and the mod-B surfaces.

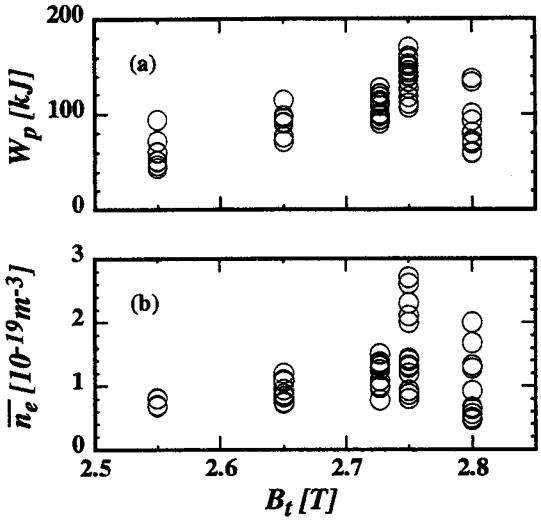

Fig. 2 Magnetic field dependences (a) stored energy and (b) line averaged plasma density. The data are ataken from the shots sustained by ICRF heating.

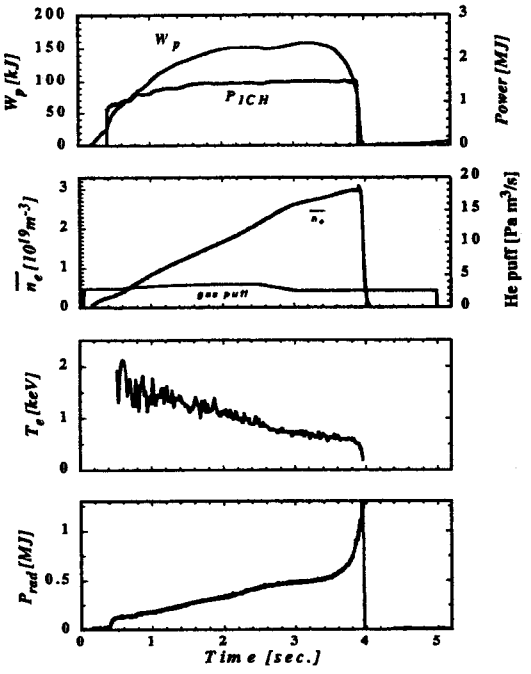

Fig. 3 Discharge waveforms: from the top stored energy and ICRF Power, line averaged electron density, electron temperature, and radiated power are shown.

of the injected ICRF heating power. At the end of the discharge (3.5 s) the radiated power was abruptly increased, indicating the operational density limit of ICRF heated plasma. This density is 83 % of the limit density deduced from the density limit scaling of the helical system [10]. It is noted that the operational density limit of the NBI heated plasma in the LHD is higher than the scale [10] giving $4\sim5\times10^{19}$ m^{-3} [11,12] for the same heating power. The density limit of ICRF sustained plasmas is thus about one half of the NBI density limit of the LHD. The difference in the operational density limits between the ICRF- and NBI-heated plasmas may be attributed to the difference in the amount of the impurity ions between them.

The energy confinement time, i.e., the performance of the ICRF heated plasma is the same as that of the NBI heated plasma, after the optimizations described in this and the next section are made.

3. The Dependence of the Heating Performance on the Magnetic Axis Position

It is known that the drift orbits of trapped ions are improved in the inward shifted magnetic configuration in the LHD. Accordingly, the 5-D Monte Carlo simulation predicts an improvement of the ICRF heating performance as the magnetic axis is shifted inward [13].

The dependence of the performance of the ICRF heating on the magnetic axis shift was investigated, applying ICRF on the NBI target plasma. A comparison was made in the case of the two different magnetic axes, R_{ax} = 3.6 m and R_{ax} = 3.75 m. Time evolutions of the plasma stored energy, the injected ICRF power and the absorbed NBI power are shown in Fig. 4. The NBI power 0.9 MW and the line-average electron density 1.0×10^{19} m^{-3} were the same for these plasma discharges. The absorbed ICRF heating powers (f = 38.47 MHz) were 0.84 MW and 0. 45 MW for the two cases of R_{ax} = 3.6 m and R_{ax} = 3.75 m, respectively. The achieved plasma stored energies were 210 kJ and 100 kJ respectively at their flat tops in the ICRF heating period. The energy confinement times normalized to ISS95 [14] scaling are 1.46 and 0.95 for the two cases of R_{ax} = 3.6 m and R_{ax} = 3.75 m, respectively. This indicates that the performance of ICRF heating is better with an inward shifted configuration. However, it has to be remembered that the energy confinement time is improved with an inward shift of the axis even with NBI [15], where energetic particles are passing particles and would be affected less by the change of the orbit of trapped particles.

Figure 5 shows the NBI data taken from the neighboring discharges; the wall conditions were similar to these in the present experiment and the magnetic axis was varied in a wider range from 3.6 m to 4.0 m. The stored energy (Fig. 5(a)) and the normalized energy confinement time (Fig. 5(b)) in the inward shifted configuration were confirmed to be larger than those in the outward-shifted configurations. Thus, the

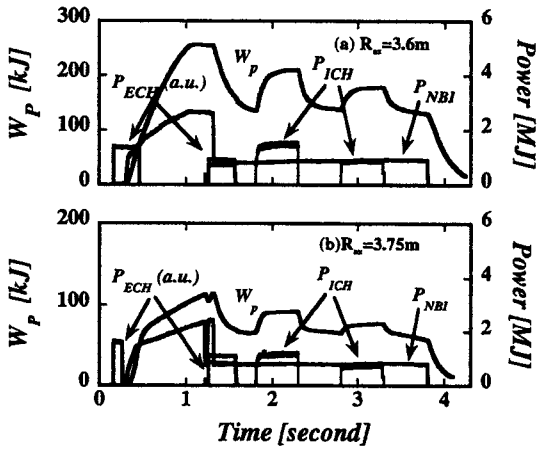

Fig. 4 Time evolutions of the plasma parameters. The magnetic axis is located at (a) R_{ax} = 3.6 m (b) R_{ax} = 3.75 m.

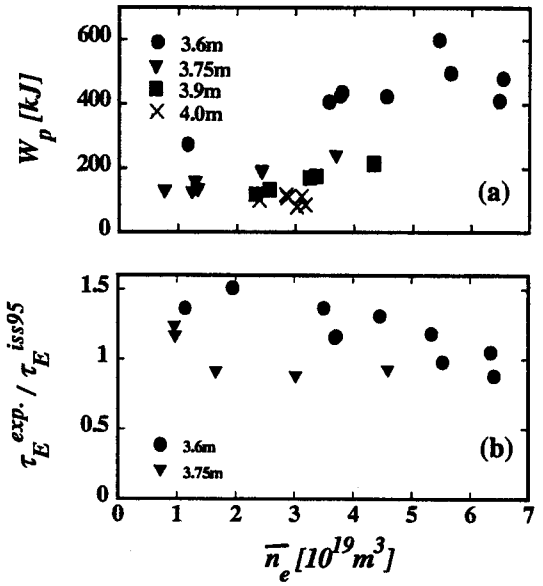

Fig. 5 The dependences of W_p and the normalized energy confinement time τ_E on the magnetic axis position. The magnetic field strength was B_t / R_{ax} = 2.75 T / 3.6 m, 2.64 T / 3.75 m, 2.54 T / 3.9 m and 2.48 T / 4.0 m on the axis.

improvement of the performance of the ICRF heating should be attributed predominantly to the improved confinement of the bulk plasma.

In order to distinguish the effect of improved drift orbits of high energy ions on the overall performance in the inward-shifted configuration from that of bulk plasma, the energy distribution was measured with the NDD (Natural Diamond Detector) [16] during the first ICRF pulse shown in Fig. 6. The second ICRF pulse is of a different frequency (f = 40.47 MHz) and is not analyzed in this paper. The high-energy ions are found to extend up to 200 keV. The tail temperature T_{tail} was determined in the energy range from 50 keV to 150 keV to be T_{tail} = 25 keV and T_{tail} = 22 keV for R_{ax} = 3.6 m and R_{ax} = 3.75 m, respectively.

On the other hand, the effective temperature T_{eff} is calculated using the Stix formula [6,17]

$$T_{eff} \cong T_e \left(1 + \frac{P_{abs}\, 2\tau_s}{3 n_H V_h T_e}\right). \qquad (1)$$

Here, T_e, P_{abs}, τ_s, n_H and V_h are the electron temperature, the RF power absorbed by high-energy ions, the ion energy slowing-down time, the minority proton density and the heating volume, respectively. The following plasma parameters are used in the calculation; T_{e0} = 2.0 keV and n_H/n_e = 9 % for R_{ax} = 3.6 m and T_{e0} = 1.6 keV and n_H/n_e = 4 % for R_{ax} = 3.75 m. The heating volume V_h is 14 % of the total plasma volume V_{LHD} (= 30 m^3) in a theoretical estimation [18], which may be taken as the minimal estimate.

The effective temperature is calculated as 38 keV and 32 keV for R_{ax} = 3.6 m and R_{ax} = 3.75 m, respectively. The ratios of the tail temperature to the effective temperature were 0.66 and 0.69 for R_{ax} = 3.6 m and R_{ax} = 3.75 m, respectively, values which are close to each other. In a more systematic analysis, the confinement time of the high-energy ions τ_h is estimated assuming the following equation:

$$\frac{1}{\tau_h} = \frac{1}{\tau^{exp.}} - \frac{1}{\tau_S} = \frac{2P_{abs}}{3n_H V_h} \frac{1}{T_{eff}^{exp.}} - \frac{1}{\tau_S}. \qquad (2)$$

The τ_h is estimated from Eq. (2) to be 0.041sec and 0.026 sec for R = 3.6 m and 3.75 m, respectively, as the specific volume V_h = 0.14 V_{LHD} is quoted. However, these values are unacceptably small; since the overall performance of the ICRF heating is comparable to that of NBI, τ_h has to be a few times larger than that of the slowing down time which is of the order of 0.1 sec. If the plasma volume is taken as V_h = 0.3 V_{LHD}, the τ_h is estimated to be 0.27 sec and 0.13 sec for R = 3.6 m and 3.75 m, respectively. This analysis suggests that the confinement of high-energy particles is better with R = 3.6 m than with 3.75 m. However, a more detailed analysis is required in order to determine the effect of the magnetic axis shift on the performance of ICRF heating via the improvement of orbits of the high-energy particle, because of the possible difference in the V_h between the two cases.

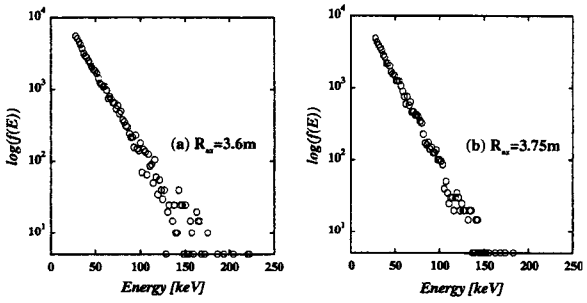

Fig. 6 Energy distributions of the high energy ions measured by NDD on the different magnetic axes: (a) R_{ax} = 3.6 m (b) R_{ax} = 3.75 m.

4. Conclusion

The performance of the ICRF heating was studied in various magnetic configurations. The location of the ion cyclotron layer was one of the key parameters for optimizing the ICRF heating. The best performance of the ICRF heating was observed when the cyclotron resonance layer locates crossing the saddle point area of the mod-B surface in the LHD magnetic configuration. In this optimized configuration, the electron density of 2.7×10^{19} m^{-3} was achieved attaining 83 % of the density limit predicted by the scaling obtained from the medium size helical devices. In the experiment shifting the magnetic axis, it was found that the global performance of ICRF heating was improved in the inward shifted configuration. The improvement is attributed to the improved energy confinement of bulk ions to a large degree. The confinement time of high-energy particles was also evaluated from the energy distribution function measured with NDD. The experimental result suggested that the volume of wave-particle interaction is larger than that estimated from a wave propagation code. With an assumed larger effective volume, the analysis gives reasonable values for the confinement times of high-energy particles and indicates its improvement in the inward-shifted case. However, there still remains an ambiguity due to the possible difference in the RF interaction volumes.

Acknowledgements

The authors thank all the scientists and the technical staff at the National Institute for Fusion Science for operation of the LHD device.

Reference

[1] T. Mutoh *et al.*, Nuclear Fusion **24**, 1003 (1984).
[2] R. Kumazawa *et al.*, (proc.21st European Conference on Controlled Fusion and Plasma Physics, 1994), part-II, p.1000–1003.
[3] R. Kumazawa *et al.*, proc. 13th Topical Conference on Applications of Radio Frequency Power to Plamas, AIP Conference Proceedings **485**, p.160–163 (1999).
[4] T. Mutoh *et al.*, Plasma Physics and Controlled Fusion **42**. 265 (2000).
[5] M. Fujiwara *et al.*, Plasma Phys. Controlled Fusion **41**, 157 B (1999).
[6] R. Kumazawa, T. Mutoh *et al.*, Physics of Plasmas **8**, 2139 (2001).
[7] T. Mutoh, R. Kumazawa, T. Seki *et al.*, Phys. Rev. Lett. **85**, 4530 (2000).
[8] T. Watari, T. Mutoh *et al.*, Nuclear Fusion **41**, 325 (2001).
[9] T. Watari, Plasma Phys. Control. Fusion **40**, A13 (1998).
[10] S. Sudo, Y. Takeiri, H. Zushi *et al.*, Nuclear Fusion **30**, 11 (1990).
[11] M. Fujiwara, K. Kawahata, N. Ohyabu *et al.*, Nuclear Fusion **41**, 1355 (2001).
[12] K. Nishimura, Annual Report of NIFS Apr. 2000 – Mar. 2001 p14.
[13] S. Murakami *et al.*, Nucl. Fusion **39**, 1165 (1999).
[14] U. Stroth *et al.*, Nuclear Fusion **36**, 1063 (1996).
[15] H. Yamada, A. Komori *et al.*, in proc. of 28th European Conference on Controlled Fusion and Plasma Physics, Madeira, 2001.
[16] A.V. Krasilnilov, Nuclear Fusion **42**, 1–9 (2002).
[17] T.H. STIX, Nuclear Fusion **15**, 737 (1975).
[18] K. Saito, R. Kumazawa and T. Mutoh, Nuclear Fusion **41**, 1021 (2001).